Inorganic Chemistry

Article

pubs.acs.org/IC

Four New Actinide Chalcogenides $Ba_2Cu_4USe_6$, $Ba_2Cu_2ThSe_5$, $Ba_2Cu_2USe_5$, and $Sr_2Cu_2US_5$: Crystal Structures and Physical Properties

Adel Mesbah,[†,‡] Jai Prakash,[†] Jessica C. Beard,[†] Sébastien Lebègue,[§] Christos D. Malliakas,[†] and James A. Ibers*[,†]

[†]Department of Chemistry, Northwestern University, 2145 Sheridan Road, Evanston, Illinois 60208-3113, United States

[‡]ICSM, UMR 5257 CEA/CNRS/UM2/ENSCM, Site de Marcoule—Bât. 426, BP 17171, 30207 Bagnols-sur-Cèze cedex, France

[§]Laboratoire de Cristallographie, Résonance Magnétique et Modélisations (CRM2, UMR CNRS 7036), Institut Jean Barriol, Université de Lorraine, BP 239, Boulevard des Aiguillettes, 54506 Vandoeuvre-lès-Nancy, France

Supporting Information

ABSTRACT: Four new actinide chalcogenides—namely, $Ba_2Cu_4USe_6$, $Ba_2Cu_2ThSe_5$, $Ba_2Cu_2USe_5$, and $Sr_2Cu_2US_5$—were synthesized via solid-state methods at 1173 K. Single-crystal X-ray diffraction studies show that $Ba_2Cu_4USe_6$ crystallizes in a new structure type in space group C_{2h}^5–$P2_1/c$ of the monoclinic system, whereas the three other compounds are isostructural and adopt the $Ba_2Cu_2US_5$ structure type in space group C_{2h}^3–$C2/m$, also of the monoclinic system. These Ak/Cu/An/Q structures (Ak = alkaline-earth metal; An = actinide; Q = chalcogen) have no short Q–Q interactions and, hence, are charge-balanced with Ak^{2+}, Cu^{1+}, An^{4+}, and Q^{2-}. Crystal structures of all these compounds are two-dimensional and feature layers that are separated by Ba^{2+} cations. The compositions of these layers differ. In the structure of $Ba_2Cu_4USe_6$, the $^2_\infty[Cu_4USe_6^{4-}]$ layers comprising USe_6 octahedra and $CuSe_4$ tetrahedra stack perpendicular to the *a*-axis. These $^2_\infty[Cu_4USe_6^{4-}]$ layers show short Cu–Cu interactions. In the three isostructural $Ak_2Cu_2AnQ_5$ compounds, AnQ_6 octahedra and CuQ_4 tetrahedra are connected along the *c*-axis in the sequence "*...oct tet tet oct tet tet...*" to form the $^2_\infty[Cu_2AnQ_5^{4-}]$ layers. Resistivity, optical, and DFT calculations show semiconducting behavior for these compounds.

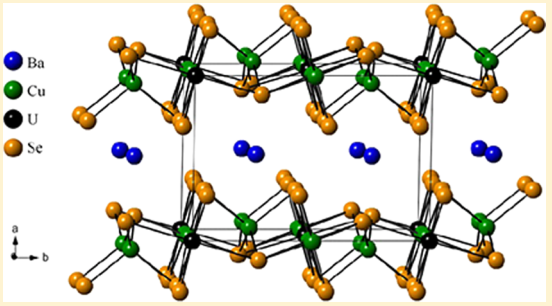

INTRODUCTION

In the last few decades, a variety of solid-state compounds have been synthesized by combining a 5f element (An = actinide) and a d-element (M = transition metal). This combination often leads to very interesting compounds with unprecedented crystal structures and exciting properties such as superconductivity and magnetism.[1−7] Additions of a chalcogen (Q = S, Se, or Te) to these 5f/d compounds to form multinary materials have also been explored by solid-state chemistry.[8−11] The majority of such compounds were synthesized by high-temperature solid-state methods involving direct combination of elements[12] or the use of the molten flux method.[13] Many of these actinide chalcogenides were discovered by exploratory syntheses. Examples of ternary compounds include MU_8Q_{17} (M = V, Ti, Cr, Co, Sc and Q = S, Se),[14−20] MUQ_3 (M = V, Cr, Sc, Ni, Co, Fe),[16,21−25] $Cu_2U_3Q_7$ (Q = S, Se),[26] and CuU_2Te_6;[27] examples of quaternary compounds include $AMUQ_3$ (A = alkali metal),[11] $A_2Pd_3UQ_6$,[28] $Cs_2M_2U_6Q_{15}$ (M = Ti, Cr, Q = Se, Te),[29] $A_6Cu_{12}U_2S_{15}$,[30] $Tl_3Cu_4USe_6$,[31] and $Tl_2Ag_2USe_4$.[31]

More recently, our group has focused on the syntheses and properties of alkaline-earth metal (Ak) actinide chalcogenides, as their chemistry is less developed than that of their alkali-metal counterparts. Exploration of quaternary Ak/M/An/Q systems has resulted in the discovery of new compounds such as Ba_3MUQ_6 (M = Mn, Fe, Ag; Q = S, Se),[32] $Ba_9Ag_{10}U_4S_{24}$,[33] $Ba_4Cr_2US_9$,[34] $Ba_8Hg_3U_3S_{18}$,[35] $Ba_2Cu_2AnS_5$ (An = Th, U),[36,37] $Ba_8PdU_2Se_{12}(Se_2)_2$,[38] and Ba_2MAnTe_7 (M = Ti, Cr; An = Th, U).[39] Here, we report the syntheses, structures, selected physical properties, and theoretical calculations for the four new compounds $Ba_2Cu_4USe_6$, $Ba_2Cu_2USe_5$, $Ba_2Cu_2ThSe_5$, and $Sr_2Cu_2US_5$.

EXPERIMENTAL METHODS

Syntheses and Analyses. *Caution! ^{232}Th and depleted U are α-emitting radioisotopes and, as such, are considered a health risk. Their use requires appropriate infrastructure and personnel trained in the handling of radioactive materials.*

All the starting reactants except U were used as supplied: Ba (Johnson Matthey, 99.5%), Sr (Aldrich, 99%), S (Mallinckrodt, 99.6%), Se (Cerac, 99.999%), Th (P Biomedicals, LLC 99.1%), Cu (Aldrich, 99.5%), CsCl (Aldrich, 99.9%). The depleted U turnings (IBI Laboratories) were powdered using a modification[40] of the previous hydridization procedure.[41] Each reaction mixture was loaded

Received: July 13, 2015
Published: September 11, 2015

DOI: 10.1021/acs.inorgchem.5b01566
Inorg. Chem. 2015, 54, 9138−9145

into a 6-mm carbon-coated fused-silica tube inside an Ar-filled drybox The tube was then evacuated to 10^{-4} Torr, flame-sealed, and placed in a computer-controlled furnace. The tube was heated to 1173 at 18 K/h, kept there for 96 h, cooled to 673 at 2.5 K/h, and then cooled to 298 at 31 K/h. The resultant products were opened under ambient conditions. They were analyzed by energy-dispersive X-ray analysis (EDX) with the use of a Hitachi S3400 scanning electron microscope (SEM). The products appear to be stable for few weeks under ambient conditions.

Synthesis of $Ba_2Cu_4USe_6$. Black irregular block-shaped crystals of $Ba_2Cu_4USe_6$ (Ba:Cu:U:Se ≈ 2:4:1:6) were obtained by the reaction of Ba (35 mg, 0.255 mmol), Cu (~5 mg, 0.31 mmol), U (20.2 mg, 0.085 mmol), and Se (40.13 mg, 0.508 mmol) in 50 mg of CsCl used as a flux. Two additional compounds $CsCuUSe_3$ (Cs:Cu:U:Se ≈ 1:1:1:3)[42] and UOSe (U:Se ≈ 1:1)[43] were observed as secondary products.

Synthesis of $Ba_2Cu_2ThSe_5$. Orange-black crystals of $Ba_2Cu_2ThSe_5$ (Ba:Cu:Th:Se ≈ 2:2:1:5) were obtained by the combination of the elements Ba (35 mg, 0.255 mmol), Cu (10 mg, 0.157 mmol), Th (19.72 mg, 0.085 mmol), and Se (40.13 mg, 0.508 mmol). Unreacted Cu metal was a byproduct.

Synthesis of $Ba_2Cu_2USe_5$. Black crystals of $Ba_2Cu_2USe_5$ (Ba:Cu:U:S ≈ 2:2:1:5) were obtained by the reaction of Ba (23.077 mg, 0.168 mmol), Cu (21.357 mg, 0.336 mmol), U (20 mg, 0.0840 mmol), and Se (39.807 mg, 0.504 mmol) in an excess of CsCl (100 mg) flux. Plate-shaped crystals of UOSe[43] and reddish BaSe (Ba:Se ≈ 1:1) crystals were observed as minor byproducts.

Synthesis of $Sr_2Cu_2US_5$. Black single crystals of $Sr_2Cu_2US_5$ (Sr:Cu:U:S ≈ 2:2:1:5) were obtained by the reaction of Sr (14.72 mg, 0.168 mmol), Cu (21.31 mg, 0.335 mmol), U (20 mg, 0.084 mmol), and S (16.16 mg, 0.504 mmol) in an excess of CsCl (100 mg) flux. UOS[44] and yellow crystals of SrS (Sr:S ≈ 1:1) were minor byproducts.

Crystal Structure Determinations. Single-crystal X-ray diffraction data were collected at 100(2) K on a Bruker APEX2 Kappa diffractometer equipped with graphite-monochromatized Mo Kα radiation (λ = 0.71073 Å). The data-collection strategy obtained by the algorithm COSMO in the APEX2 package comprised ω and φ scans.[45] The step size was 0.3°, and exposure time was 10 s/frame. Data were indexed, refined, and integrated with the use of SAINT program in the APEX2 package.[45] Numerical face-indexed absorption corrections were applied with the use of the program SADABS.[46] Precession images created from the observed data showed no evidence of modulations or superstructures. The crystal structures were solved and refined with the use of the SHELX-14 algorithms of the SHELXL program package.[46,47] The program STRUCTURE TIDY[48] in PLATON[49] was used to standardize the atomic positions. Crystal structure data and the refinement parameters are given in Table 1 and in the Supporting Information.

Resistivity Measurements. Four-probe high-temperature-dependent resistivity data were collected using a homemade resistivity apparatus equipped with a Keithley Model 2182 nanovoltmeter, a Keithley 236 source measure unit, and a high-temperature vacuum chamber controlled by a K-20 MMR system. An $I-V$ curve from 1×10^{-8} A to -1×10^{-8} A with a step of 4×10^{-9} A was measured for each temperature point from 300 K to 500 K and resistance was calculated from the slope of the $I-V$ plot. Data acquisition was controlled by custom-written software. Graphite paint (PELCO isopropanol-based graphite paint) was used for electrical contacts with Cu wires of 0.025 mm thickness (Omega). The DC current was applied along an arbitrary direction on single crystals with dimensions 0.3 mm × 0.2 mm × 0.1 mm, 0.2 mm × 0.3 mm × 0.2 mm, and 0.3 mm × 0.5 mm × 0.2 mm for $Ba_2Cu_4USe_6$, $Ba_2Cu_2USe_5$, and $Sr_2Cu_2US_5$, respectively.

Optical Measurements. Single-crystal absorption spectra for $Ba_2Cu_2ThSe_5$ were obtained at 298 K on a Hitachi U-6000 Microscopic FT spectrophotometer mounted on an Olympus Model BH2-UMA microscope. A crystal of $Ba_2Cu_2ThSe_5$ was placed on a glass slide and positioned over the light source, where the transmitted light was recorded from above. The background signal of the glass slide was subtracted from the collected intensity.

Table 1. Crystallographic Data and Structure Refinement Details for $Ba_2Cu_4USe_6$, $Ba_2Cu_2ThSe_5$, $Ba_2Cu_2USe_5$, and $Sr_2Cu_2US_5$[a]

	$Ba_2Cu_4USe_6$	$Ba_2Cu_2ThSe_5$	$Ba_2Cu_2USe_5$	$Sr_2Cu_2US_5$
space group	$C_{2h}^5-P2_1/c$	C_{2h}^3-C2/m	C_{2h}^3-C2/m	C_{2h}^3-C2/m
a (Å)	7.1783(3)	14.0702(2)	14.0378(1)	13.037(3)
b (Å)	9.7866(4)	4.2692(1)	4.2216(1)	3.9821(8)
c (Å)	8.9589(4)	9.7338(2)	9.6545(1)	9.258(1)
β (deg)	108.062(1)	115.891(1)	116.158(1)	116.73(3)
V (Å^3)	598.36(4)	526.01(1)	513.54(2)	429.27(18)
ρ (g cm^{-3})	6.886	6.494	6.691	5.421
μ (mm^{-1})	45.117	42.665	44.986	37.142
$R(F)^b$	0.028	0.025	0.015	0.014
$R_w(F_o^2)^c$	0.088	0.086	0.039	0.038

[a]For all structures, Z = 2, λ = 0.71073 Å, and T = 100(2) K. [b]$R(F) = \sum||F_o| - |F_c||/\sum|F_o|$ for $F_o^2 > 2\sigma(F_o^2)$. [c]$R_w(F_o^2) = \{\sum[w(F_o^2 - F_c^2)^2]/\sum wF_o^4\}^{1/2}$. For $F_o^2 < 0$, $w^{-1} = \sigma^2(F_o^2)$; for $F_o^2 \geq 0$, $w^{-1} = \sigma^2(F_o^2) + (qF_o^2)^2$, where q = 0.0340 for $Ba_2Cu_4USe_6$, 0.0220 for $Ba_2Cu_2ThSe_5$, 0.000 for $Ba_2Cu_2USe_5$, and 0.0149 for $Sr_2Cu_2US_5$.

The spectrophotometer was not suitable for the measurement of the black U compounds. A suitable instrument required powders, but pure powders could not be obtained.

Theoretical Calculations. These were carried out with the Vienna Ab Initio Simulation Package[50,51] implementing density functional theory[52,53] with the projector-augmented wave method.[54] The Heyd–Scuseria–Ernzerhof (HSE)[55−57] exchange-correlation potential allowing for spin polarization was used. The atom positions and cell parameters used in the calculations were taken from the experimental results. For the U compounds, the various possible magnetic orders occurring in a crystal cell were calculated, and the one with the lowest total energy was retained as the ground state. The default cutoff and a mesh of 4 × 4 × 4 k-points to sample the Brillouin zone were used to reach numerical convergence.

RESULTS AND DISCUSSION

Syntheses. In an attempt to synthesize the 2H hexagonal perovskite Ba_3CuUSe_6, the elements Ba, Cu, U, and Se in the molar ratio of ~3:1:1:6 were reacted in a CsCl flux at 1173 K. Instead of Ba_3CuUSe_6, the major product of this reaction was the new quaternary compound $Ba_2Cu_4USe_6$ (yield ≈ 70 wt %, based on Cu). The two byproducts were UOSe[43] and $CsCuUSe_3$.[42] It is surprising that $CsCuUSe_3$ formed, as the CsCl flux was not in excess. In an attempt to improve the yield, the elements in the molar ratio of 2:4:1:6 were reacted in excess CsCl flux at 1173 K. Rather than $Ba_2Cu_4USe_6$, the compound $Ba_2Cu_2USe_5$ was obtained in high yield (>80 wt % based on U), along with small amounts of binary Ak/Se compounds and

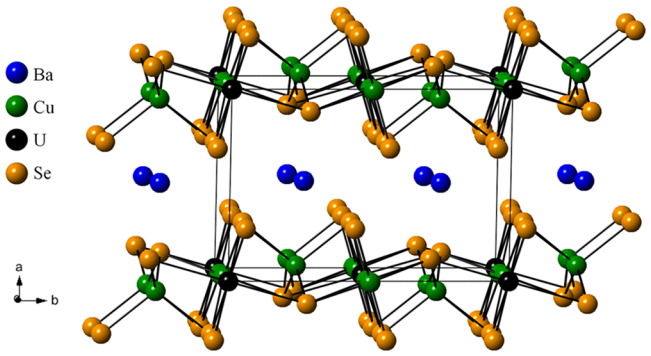

Figure 1. Crystal structure of $Ba_2Cu_4USe_6$ viewed down the c-axis.

DOI: 10.1021/acs.inorgchem.5b01566
Inorg. Chem. 2015, 54, 9138−9145

Table 2. Selected Interatomic Distances for $Ba_2Cu_4USe_6$[a]

bond pair	distance (Å)	bond pair	distance (Å)
U1−Se2	2.794(1) × 2	Ba1−Se3	3.192(1)
U1−Se3	2.827(1) × 2	Ba1−Se3	3.211(1)
U1−Se1	2.856(1) × 2	Ba1−Se2	3.267(1)
Cu1−Se3	2.396(1)	Ba1−Se1	3.372(1)
Cu1−Se1	2.606(1)	Ba1−Se3	3.385(1)
Cu1−Se2	2.396(1)	Ba1−Se2	3.423(1)
Cu1−Se1	2.611(2)	Ba1−Se1	3.434(1)
Cu2−Se3	2.433(2)	Ba1−Se2	3.485(1)
Cu2−Se2	2.445(2)	Ba1···Ba1	4.493(1)
Cu2−Se1	2.567(1)	U1···U1	6.634(1)
Cu2−Se1	2.576(1)	U1···Cu1	3.218(1) × 2
Cu1···Cu1	2.525(2)	U1···Cu2	3.331(1) × 2
Cu1···Cu2	2.650(2)	U1···Cu2	3.363(1) × 2
Cu2···Cu2	4.480(1)	Se···Se	3.823(1)

[a]All interatomic distances have been rounded to facilitate comparisons.

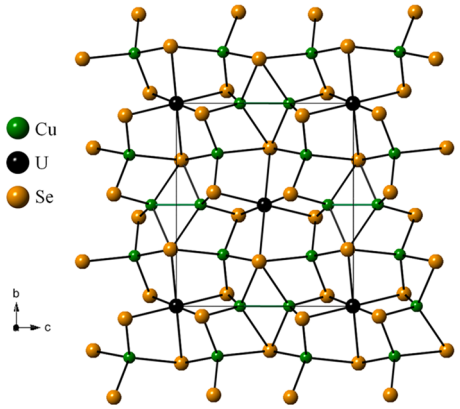

Figure 2. A projection down the *a*-axis of the $^2_\infty[Cu_4USe_6^{4-}]$ layers in the structure of $Ba_2Cu_4USe_6$.

UOSe. A similar reaction, with Sr in place of Ba, provided neither $Sr_2Cu_2USe_5$ nor $Sr_2Cu_4USe_6$; however, surprisingly, a reaction with Sr in place of Ba and S in place of Se provided $Sr_2Cu_2US_5$ in ∼80 wt % yield, along with SrS and UOS. In these reactions, the compounds UOSe and UOS arise from the etching of the fused-silica tubes. A similar reaction, with Th in place of U, did not yield $Ba_2Cu_2ThSe_5$, but the compound was obtained from the flux-free synthesis of the elements in the molar ratio of ∼3:2:1:6 at 1173 K. The byproduct was unreacted Cu.

Crystal Structure of $Ba_2Cu_4USe_6$. This compound crystallizes in a new structure type in space group C^5_{2h}−$P2_1/c$ of the monoclinic system. There are two formula units per cell.

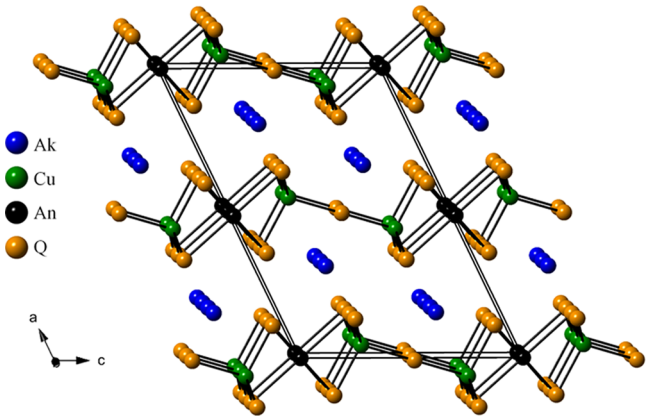

Figure 4. General view down the *b*-axis of the $Ak_2Cu_2AnQ_5$ structure.

Table 3. Selected Interatomic Distances for the $Ak_2Cu_2AnQ_5$ Compounds $Ba_2Cu_2ThSe_5$, $Ba_2Cu_2USe_5$, and $Sr_2Cu_2US_5$[a]

	Distance (Å)		
	$Ba_2Cu_2ThSe_5$	$Ba_2Cu_2USe_5$	$Sr_2Cu_2US_5$
An1−Q2	2.949(1) × 4	2.894(1) × 4	2.753(1) × 4
An1−Q1	2.882(1) × 2	2.802(1) × 2	2.668(2) × 2
Cu1−Q3	2.436(1)	2.430(1)	2.303(1)
Cu1−Q1	2.499(1) × 2	2.473(1) × 2	2.348(1) × 2
Cu1−Q2	2.500(2)	2.462(1)	2.373(2)
Ak1−Q3	3.178(1) × 2	3.165(1) × 2	2.944(1) × 2
Ak1−Q1	3.277(1) × 2	3.279(1) × 2	3.009(1) × 2
Ak1−Q2	3.490(1)	3.413(1)	3.229(1) × 2
Ak1−Q2	3.512(1) × 2	3.477(1) × 2	3.265(2)
Ak1−Q1	3.547(1)	3.621(1)	3.559(1)
Q···Q	3.832(1)	3.819(1)	3.591(1)
An1···Cu1	3.379(1)	3.335(1)	3.228(1)
Ak1···Cu1	3.770(1)	3.787(1)	3.499(1)

[a]All interatomic distances have been rounded to facilitate comparisons.

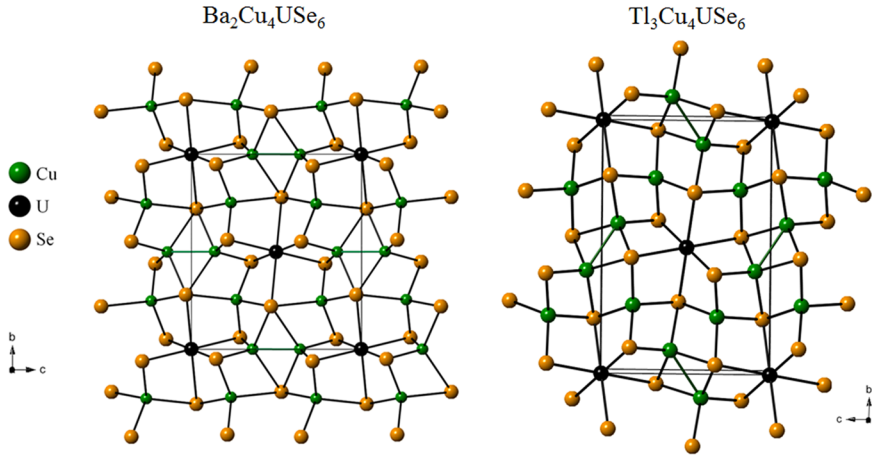

Figure 3. Comparison of the two-dimensional layers in the structures of $Ba_2Cu_4USe_6$ and $Tl_3Cu_4USe_6$.[31]

DOI: 10.1021/acs.inorgchem.5b01566
Inorg. Chem. 2015, 54, 9138−9145

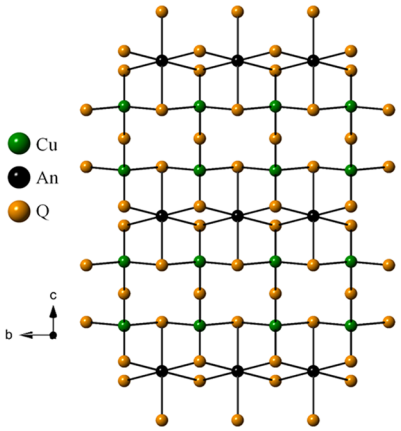

Figure 5. View down the *a*-axis of the two-dimensional layer in the structure of $Ak_2Cu_2AnQ_5$.

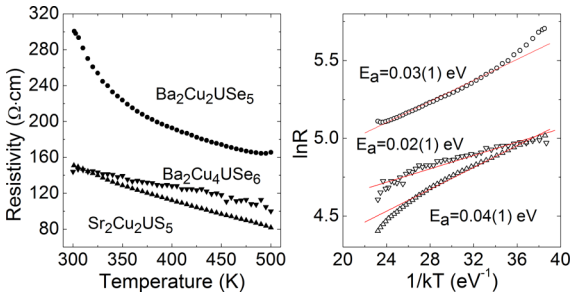

Figure 6. (Left) Resistivity as a function of temperature for $Ba_2Cu_4USe_6$, $Ba_2Cu_2USe_5$, and $Sr_2Cu_2US_5$ crystals showing semiconducting behavior. (Right) Arrhenius plots with activation energies of 0.02(1), 0.04(1), and 0.03(1) eV for $Ba_2Cu_4USe_6$, $Sr_2Cu_2US_5$, and $Ba_2Cu_2USe_5$, respectively.

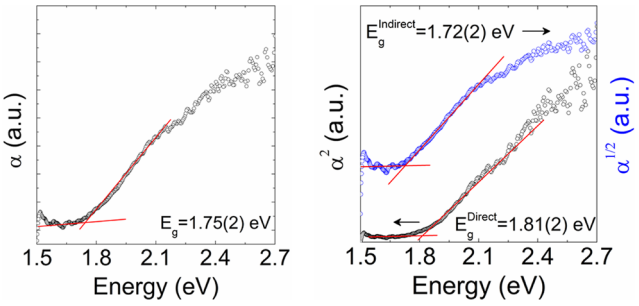

Figure 7. (Left) Optical absorptivity (α) of a $Ba_2Cu_2ThSe_5$ single crystal with a band gap of 1.75(2) eV. (Right) Plots of α^2 and $\alpha^{1/2}$ vs energy.

The asymmetric unit comprises one Ba atom, two Cu atoms, one U atom, and three Se atoms, all in general positions except for the U atom, which has site symmetry $\bar{1}$. A general projection of the structure down the *b*-axis is shown in Figure 1, and metrical data for $Ba_2Cu_4USe_6$ are given in Table 2. Each U atom is octahedrally coordinated to six Se atoms with U−Se distances of 2.794(1), 2.827(1), and 2.856(1) Å. These U−Se distances are in agreement with those found in related U^{4+} compounds in which the U atom is octahedrally coordinated: $Cs_2Pt_3USe_6$ (2.835(1)−2.881(1) Å),[28] $Cs_2Pd_3USe_6$ (2.835(1)−2.870(1) Å),[28] $Tl_2Ag_2USe_4$ (2.853(2)−2.881(1) Å),[31] and $CsCuUSe_3$ (2.826(1)−2.861(1) Å).[42]

The Cu1 atoms exhibit Cu···Cu short interactions of 2.524(1) Å and each Cu1 atom is also connected to four Se atoms (two Se1, one Se2, and one Se3) with distances of 2.606(1), 2.611(2), 2.396 (1), and 2.396(1) Å, respectively. A short Cu···Cu interaction is also observed for the related $Tl_3Cu_4USe_6$ structure (2.571(3)−2.654(3) Å).[31] The Cu2 atoms in $Ba_2Cu_4USe_6$ are surrounded by four Se atoms in a less-distorted tetrahedral geometry than for Cu1 with distances of 2.567(1), 2.576(1), 2.445(2), and 2.433(2) Å for Se1, Se1, Se2, and Se3, respectively. The shortest Cu2···Cu2 distance is 4.480(1) Å. The Cu−Se distances (2.396−2.611(1) Å) compare well with the corresponding distances in the structures of related Cu^{1+} compounds such as $Tl_3Cu_4USe_6$ (2.427(2)−2.604(2) Å),[31] $CuNdSe_2$ (2.430(1)−2.583(1) Å),[58] Cu_2SiSe_3 (2.390(1)−2.515(1) Å),[59] and $K_3CuNb_2Se_{12}$ (2.388(1)−2.504(1) Å).[60]

The Ba^{2+} cations are coordinated to eight Se atoms with Ba−Se distances ranging from 3.192(1) Å and 3.485(1) Å. These compare well with those found in $BaAuGdSe_3$ (3.206(1)−3.574(1) Å),[61] in which the coordination of Ba is similar.

The crystal structure of $Ba_2Cu_4USe_6$ consists of $^2_\infty[Cu_4USe_6^{4-}]$ infinite layers perpendicular to the *a*-axis separated by Ba^{2+} cations (Figure 2). The composition of the $^2_\infty[Cu_4USe_6^{4-}]$ layers shows similarities to the $^2_\infty[Cu_4USe_6^{3-}]$ layers in the U^{5+} compound $Tl_3Cu_4USe_6$ (Figure 3).[31] In each, the USe_6 octahedra are surrounded by $CuSe_4$ tetrahedra. However, in $Ba_2Cu_4USe_6$, the apical Se atoms of the USe_6 octahedra are connected to four Cu atoms and all equatorial Se atoms are bonded to two Cu atoms. In contrast, in $Tl_3Cu_4USe_6$, the apical Se atoms of the USe_6 octahedra are connected to three Cu atoms while two equatorial Se atoms are bonded to two Cu atoms and the remaining two Se atoms are bonded to three Cu atoms.[31]

Because the shortest Se···Se distance is 3.823(1) Å, $Ba_2Cu_4USe_6$ is charge-balanced as Ba^{2+}, Cu^{1+}, U^{4+}, Se^{2-}.

Crystal Structures of $Ba_2Cu_2ThSe_5$, $Ba_2Cu_2USe_5$, and $Sr_2Cu_2US_5$. These isostructural compounds with general formula $Ak_2Cu_2AnQ_5$ adopt the $Ba_2Cu_2US_5$[37] structure type in space group C^3_{2h}−*C*2/*m* of the monoclinic system. There are two formula units per cell. The asymmetric unit contains one Ak (*m* symmetry site), one Cu (*m*), one An (2/m), and three Q atoms (Q1 (*m*), Q2 (*m*), and Q3 (2/*m*)). The crystal structure of $Ak_2Cu_2AnQ_5$ viewed down the *b*-axis is shown in Figure 4, and metrical data are given in Table 3. The structure comprises AnQ_6 octahedra and CuQ_4 distorted tetrahedra. The structure is two-dimensional with $^2_\infty[Cu_2AnSe_5^{4-}]$ layers perpendicular to the *a*-axis separated by the Ak cations (Figure 4). Each Ak atom is coordinated to eight Se atoms in a bicapped trigonal-prismatic geometry. The AnQ_6 octahedra and CuQ_4 tetrahedra are connected in the sequence *...oct tet tet oct tet tet oct...* in the [001] direction (Figure 5).

Th−Se distances of 2.882 (1) and 2.949(1) Å in $Ba_2Cu_2ThSe_5$ are in agreement with those found in $TlCuThSe_3$ (2.884(1)−2.906(1) Å)[62] and ThSe (2.932(1) Å)[63] with Th^{4+} in octahedral geometry. As expected, these distances are longer than the corresponding U−Se distances, because of the actinide contraction. The U−Se interatomic distances of 2.802(1) Å and 2.894(1) Å in $Ba_2Cu_2USe_5$ are also normal. Compare these with those in related structures: $Ba_2Cu_4USe_6$, 2.794(1)−2.856(1) Å; $Cs_2Pt_3USe_6$, 2.835(1)−2.881(1) Å;[28] $Cs_2Pd_3USe_6$, 2.835(1)−2.870(1) Å;[28] $Tl_2Ag_2USe_4$, 2.853(2)−2.881(1) Å;[31] and $CsCuUSe_3$, 2.826(1)−2.861(1) Å.[42] The Cu−Se distances in $Ba_2Cu_2ThSe_5$ (2.436(1)−2.500(2) Å) and $Ba_2Cu_2USe_5$ (2.430(1)−2.473(1) Å) compare well with those in known Cu^{1+} structures such as $KCuUSe_3$ (2.446(1)−2.514(1) Å),[64]

DOI: 10.1021/acs.inorgchem.5b01566
Inorg. Chem. 2015, 54, 9138−9145

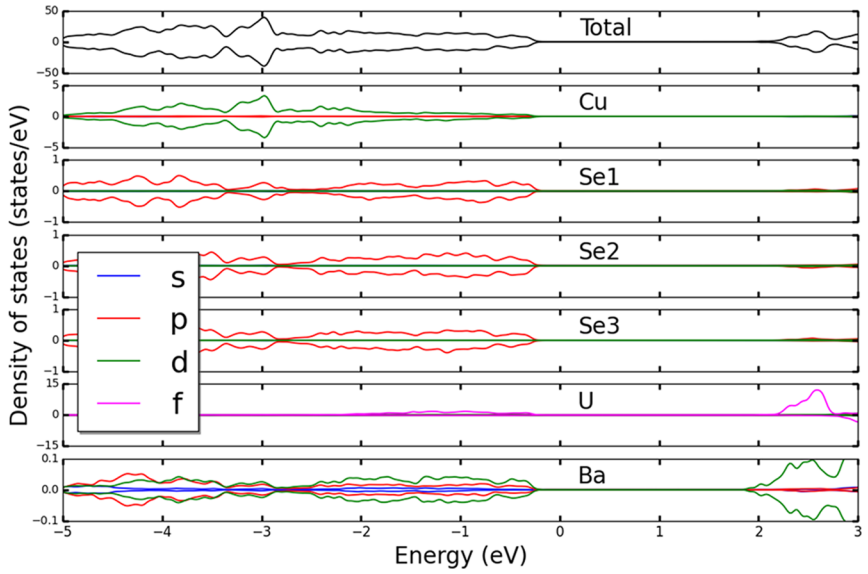

Figure 8. Total (upper plot) and partial density of states (lower plots) of $Ba_2Cu_4USe_6$.

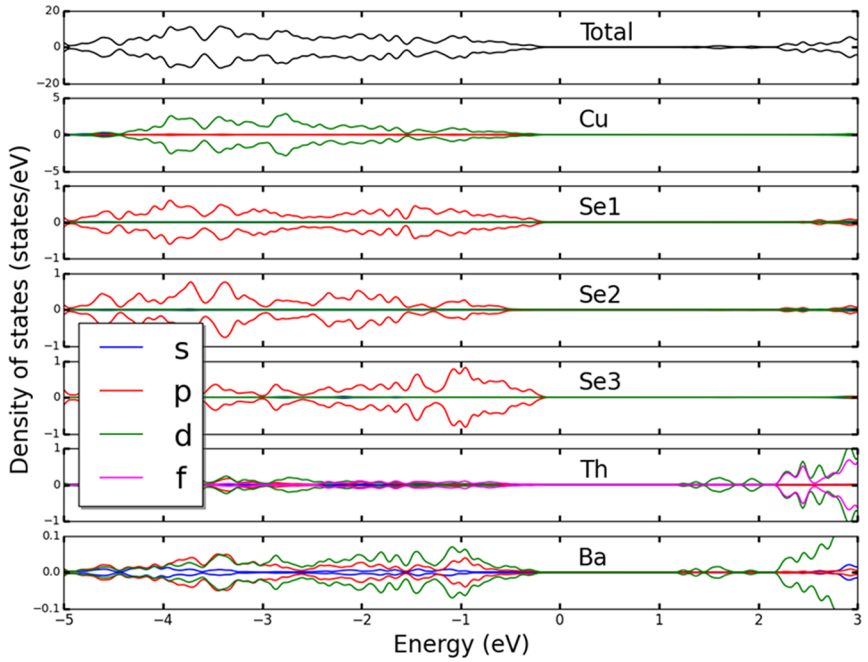

Figure 9. Total (upper plot) and partial density of states (lower plots) of $Ba_2Cu_2ThSe_5$.

KCu_2NbSe_4 (2.426(1)−2.440(1) Å),[65] $K_2CuNbSe_4$ (2.454 Å),[60] and Cu_2SiSe_3 (2.390(1)−2.515(1) Å).[59] Ba−Se distances range between 3.165(1) Å and 3.621(1) Å in $Ba_2Cu_2AnSe_5$; these may be compared with those found in $BaAuGdSe_3$ (3.206(1)−3.574(1) Å)[61] with similar eight-coordinated Ba^{2+}.

U−S distances of 2.668(2) Å and 2.753(1) Å in $Sr_2Cu_2US_5$ are comparable with U^{4+}−S distances of US_6 octahedra in Ba_3FeUS_6 (2.712(1) Å),[32] $Ba_2Cu_2US_5$ (2.673(2)−2.770(1) Å),[37] $BaUS_3$ (2.677(1)−2.696(1) Å),[66] $Ba_4Cr_2US_9$ (2.688(5)−2.764(4) Å),[34] $CsCuUS_3$ (2.706(1)−2.723(1) Å),[67] $RbCuUS_3$ (2.708(1)−2.718(1) Å),[67] and $KCuUS_3$ (2.714(1)−2.717(1) Å).[67] The Cu−S distances (2.303(1)−2.373(2) Å) in $Sr_2Cu_2US_5$ are also in agreement with those in related compounds, such as $Ba_2Cu_2US_5$ (2.305(1)−2.381(1) Å),[37] $KCuUS_3$ (2.321(1)−2.405(1) Å,[67] $CsCuUS_3$ (2.327(1)−2.413(1) Å),[67] and $RbCuUS_3$ (2.324(1)−2.407(1) Å)[67] containing tetrahedral Cu^{1+} cations. The Sr−S distances in $Sr_2Cu_2US_5$ range between 2.944(1) Å and 3.559(1) Å; those in SrU_2S_5[68] range between 2.965(1) Å and 3.589(1) Å.

The assignment of the formal oxidation states is straightforward for these $Ak_2Cu_2AnQ_5$ compounds, because of the absence of any short Q−Q interactions. The shortest Se···Se and S···S interactions are 3.832(1), 3.819(1), and 3.592(1) Å for $Ba_2Cu_2ThSe_5$, $Ba_2Cu_2USe_5$, and $Sr_2Cu_2US_5$, respectively. Thus, charge balance is achieved with Ak^{2+}, Cu^{1+}, An^{4+}, and Q^{2-}.

Resistivity Studies. The temperature dependences of the resistivities of $Ba_2Cu_4USe_6$, $Ba_2Cu_2USe_5$, and $Sr_2Cu_2US_5$ show semiconducting behavior in the temperature range of 300−500 K (Figure 6). The resistivities at 298 K are ∼150 Ω cm for both $Ba_2Cu_4USe_6$ and $Sr_2Cu_2US_5$ and ∼300 Ω cm for $Ba_2Cu_2USe_5$. The resistivities decrease weakly as the temperature increases

DOI: 10.1021/acs.inorgchem.5b01566
Inorg. Chem. 2015, 54, 9138−9145

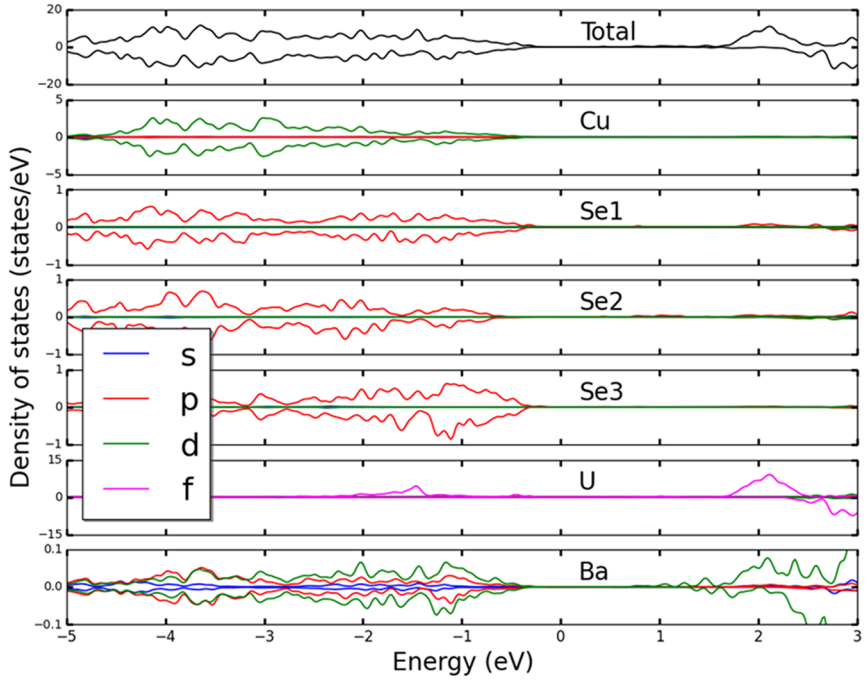

Figure 10. Total (upper plot) and partial density of states (lower plots) of $Ba_2Cu_2USe_5$.

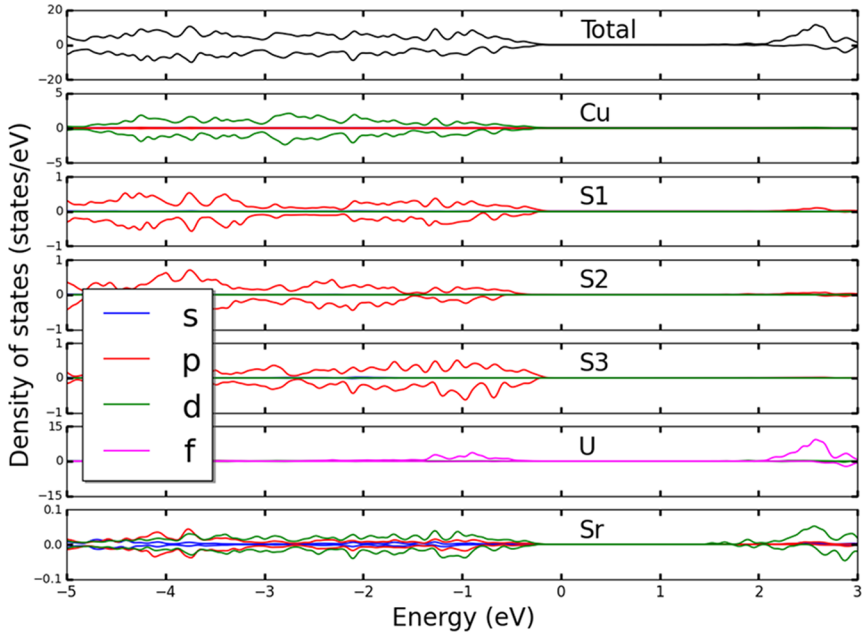

Figure 11. Total (upper plot) and partial density of states (lower plots) of $Sr_2Cu_2US_5$.

and, at 500 K, are ∼100, 80, and 165 Ω cm for $Ba_2Cu_4USe_6$, $Sr_2Cu_2US_5$, and $Ba_2Cu_2USe_5$, respectively. The corresponding activation energies, as estimated from Arrhenius plots (see Figure 6) are 0.02(1), 0.04(1), and 0.03(1) eV.

Optical Studies. The absorptivity (α) at 298 K of a single crystal of $Ba_2Cu_2ThSe_5$ (Figure 7) shows a broad band gap transition at 1.75(2) eV. Analysis of α^2 and $\alpha^{1/2}$ as a function of energy (Figure 7) gives a direct band gap of 1.81(2) eV and an indirect band gap of 1.72(2) eV. This wide energy gap is consistent with the dark red color of the crystals.

DFT Calculations. The total (upper plot) and partial (lower plots) density of states (DOS) of $Ba_2Cu_4USe_6$ are shown in Figure 8. A gap of 2.0 eV is seen in the total DOS and the compound is found to be antiferromagnetic, with most of the magnetic moment carried by the U atoms with almost no induced polarization on the neighboring atoms. The top of the valence states is derived mainly from Se-p, Cu-d, and U-f states, while the bottom of the conduction states is made up of U-f states.

The DOS of $Ba_2Cu_2ThSe_5$ is presented in Figure 9. As expected, $Ba_2Cu_2ThSe_5$ is found to be nonmagnetic, as seen by the symmetric partial density of states for each atom. The band gap is 1.2 eV, compared with the experimental value of 1.75 eV. The states immediately below the Fermi level are composed of Se-p and Cu-d, while the states just above the Fermi level correspond to Th-d and Ba-d states.

DOI: 10.1021/acs.inorgchem.5b01566
Inorg. Chem. 2015, 54, 9138−9145

The DOS of $Ba_2Cu_2USe_5$ is shown in Figure 10. According to our calculations, this compound has a band gap of 0.4 eV. The magnetic moment carried by the U atoms is clearly seen from the corresponding DOS, which is not symmetric with the spin. This magnetic moment induces a small spin polarization on some other atoms, such as Se3 and Ba. The top of the valence states is made of Se-p and U-f states, while the bottom of the conduction states corresponds to Se-p, Ba-d, and U-f states.

$Sr_2UCu_2S_5$ has a gap of 1.5 eV, as shown by the corresponding DOS in Figure 11. The magnetic moment on the U atoms has a significant influence on the DOS plots of atoms Sr, S2, and S3. The top of the valence states corresponds to S-p, Cu-d, and U-f states, while the bottom of the conduction states are derived from Sr-d and U-f states.

The 5f compounds $Ba_2Cu_4USe_6$, $Ba_2Cu_2ThSe_5$, $Ba_2Cu_2USe_5$, and $Sr_2Cu_2US_5$ have complex structures and thus present a challenge to DFT calculations. Thus, comparing the calculated band gaps between different structures, e.g., those of $Ba_2Cu_4USe_6$ and $Ba_2Cu_2USe_5$, is not justified. It may not be justified to make comparisons within a given structure type, but it is at least encouraging that the calculated band gaps of 0.4 and 1.5 eV for $Ba_2Cu_2USe_5$ and $Sr_2Cu_2US_5$ change in the direction expected for the more-ionic sulfide.

CONCLUSIONS

Exploratory syntheses in the Ak/Cu/An/Q system have resulted in the discovery of four new quaternary compounds, namely $Ba_2Cu_4USe_6$, $Ba_2Cu_2ThSe_5$, $Ba_2Cu_2USe_5$, and $Sr_2Cu_2US_5$. $Ba_2Cu_4USe_6$ crystallizes with two formula units per cell in a new structure type in space group C_{2h}^5–$P2_1/c$ of the monoclinic system. This compound has a two-dimensional crystal structure, with infinite layers of $^2_\infty[Cu_4USe_6^{4-}]$ perpendicular to the *a*-axis. Resistivity measurements indicate that the compound is a semiconductor with an activation energy of 0.03(1) eV. Density functional theory (DFT) calculations predict a band gap of 2.0 eV.

The other three compounds—$Ba_2Cu_2ThSe_5$, $Ba_2Cu_2USe_5$, and $Sr_2Cu_2US_5$—are isostructural and crystallize in the $Ba_2Cu_2US_5$ structure type in space group C_{2h}^3–$C2/m$, also of the monoclinic system. The two-dimensional layers of $^2_\infty[Cu_2AnQ_5^{4-}]$ result from the connections of AnQ_6 octahedra and CuQ_4 tetrahedra in the sequence "*...oct tet tet oct tet tet...*". Resistivity measurements for $Ba_2Cu_2ThSe_5$ indicate semiconducting behavior with an activation energy of 0.02(1) eV. For $Ba_2Cu_2ThSe_5$, optical studies indicate a direct band gap of 1.81(2) eV and an indirect band gap of 1.72(2) eV. A theoretical band gap of 1.2 eV was calculated by DFT. Resistivity studies of $Ba_2Cu_2USe_5$ and $Sr_2Cu_2US_5$ confirm their semiconducting nature with small activation energies of 0.04(1) and 0.03(1) eV, respectively. DFT calculations also predict semiconducting behavior for $Ba_2Cu_2USe_5$ and $Sr_2Cu_2US_5$ with estimated band gaps of 0.4 and 1.5 eV, respectively.

ASSOCIATED CONTENT

Supporting Information

The Supporting Information is available free of charge on the ACS Publications website at DOI: 10.1021/acs.inorgchem.5b01566.

Crystallographic files for $Ba_2Cu_4USe_6$, $Ba_2Cu_2ThSe_5$, $Ba_2Cu_2USe_5$, and $Sr_2Cu_2US_5$ (CIF)

AUTHOR INFORMATION

Corresponding Author

*E-mail: ibers@chem.northwestern.edu.

Notes

The authors declare no competing financial interest.

ACKNOWLEDGMENTS

Use was made of the IMSERC X-ray Facility at Northwestern University, supported by the International Institute of Nanotechnology (IIN). C.D.M. was supported by the U.S. Department of Energy, Office of Basic Energy Sciences, under Contract No. DE-AC02-06CH11357. S.L. acknowledges HPC resources from GENCI-CCRT/CINES (Grant No. x2015-085106). Parts of the calculations were performed in the Computing Centre of the Slovak Academy of Sciences using the supercomputing infrastructure acquired in Project Nos. ITMS26230120002 and 26210120002 (Slovak Infrastructure for High-Performance Computing) supported by the Research and Development Operational Programme funded by the ERDF.

REFERENCES

(1) Sato, N. K.; Aso, N.; Miyake, K.; Shiina, R.; Thalmeier, P.; Varelogiannis, G.; Geibel, C.; Steglich, F.; Fulde, P.; Komatsubara, T. *Nature (London, U. K.)* **2001**, *410*, 340−343.
(2) Baumbach, R. E.; Hamlin, J. J.; Janoschek, M.; Lum, I. K.; Maple, M. B. *J. Phys.: Condens. Matter* **2011**, *23*, 094222-1−094222-5.
(3) Maple, M. B. *Phys. C* **2000**, *341*−*348*, 47−52.
(4) Griveau, J.-C.; Boulet, P.; Colineau, E.; Wastin, F.; Rebizant, J. *Phys. B* **2005**, *359*−*361*, 1093−1095.
(5) Andreev, A. V.; Chernyavsky, A.; Izmaylov, N.; Sechovsky, V. *J. Alloys Compd.* **2003**, *353*, 12−16.
(6) Thompson, J. D.; Ekimov, E. A.; Sidorov, V. A.; Bauer, E. D.; Morales, L. A.; Wastin, F.; Sarrao, J. L. *J. Phys. Chem. Solids* **2006**, *67*, 557−561.
(7) Mougel, V.; Chatelain, L.; Pécaut, J.; Caciuffo, R.; Colineau, E.; Griveau, J.-C.; Mazzanti, M. *Nat. Chem.* **2012**, *4*, 1011−1017.
(8) Manos, E.; Kanatzidis, M. G.; Ibers, J. A. In *The Chemistry of the Actinide and Transactinide Elements*, 4th Edition; Morss, L. R., Edelstein, N. M., Fuger, J., Eds.; Springer: Dordrecht, The Netherlands, 2010; Vol. *6*, pp 4005−4078.
(9) Bugaris, D. E.; Ibers, J. A. *Dalton Trans.* **2010**, *39*, 5949−5964.
(10) Narducci, A. A.; Ibers, J. A. *Chem. Mater.* **1998**, *10*, 2811−2823.
(11) Koscielski, L. A.; Ibers, J. A. *Z. Anorg. Allg. Chem.* **2012**, *638*, 2585−2593.
(12) Prakash, J.; Lebègue, S.; Malliakas, C. D.; Ibers, J. A. *Inorg. Chem.* **2014**, *53*, 12610−12616.
(13) Sunshine, S. A.; Kang, D.; Ibers, J. A. *J. Am. Chem. Soc.* **1987**, *109*, 6202−6204.
(14) Ward, M. D.; Mesbah, A.; Minasian, S. G.; Shuh, D. K.; Tyliszczak, T.; Lee, M.; Choi, E. S.; Lebègue, S.; Ibers, J. A. *Inorg. Chem.* **2014**, *53*, 6920−6927.
(15) Noël, H. *C. R. Seances Acad. Sci., Ser. C* **1974**, *279*, 513−515.
(16) Noël, H. *C. R. Seances Acad. Sci., Ser. C* **1973**, *277*, 463−464.
(17) Noël, H.; Potel, M.; Padiou, J. *Acta Crystallogr., Sect. B: Struct. Crystallogr. Cryst. Chem.* **1975**, *31*, 2634−2637.
(18) Noel, H.; Troc, R. *J. Solid State Chem.* **1979**, *27*, 123−135.
(19) Oh, G. N.; Ibers, J. A. *Acta Crystallogr., Sect. E: Struct. Rep. Online* **2011**, *E67*, i46.
(20) Vovan, T.; Rodier, N. *C. R. Seances Acad. Sci., Ser. C* **1979**, *289*, 17−20.
(21) Jin, G. B.; Ringe, E.; Long, G. J.; Grandjean, F.; Sougrati, M. T.; Choi, E. S.; Wells, D. M.; Balasubramanian, M.; Ibers, J. A. *Inorg. Chem.* **2010**, *49*, 10455−10467.
(22) Andersson, Y.; Pramatus, S.; Rundqvist, S.; et al. *Acta Chem. Scand.* **1978**, *32A*, 811−813.

DOI: 10.1021/acs.inorgchem.5b01566
Inorg. Chem. 2015, 54, 9138−9145

(23) Chenevier, B.; Wolfers, P.; Bacmann, M.; Noël, H. *C. R. Acad. Sci., Sér. 2* **1981**, *293*, 649−652.
(24) Noël, H.; Padiou, J.; Prigent, J. *C. R. Seances Acad. Sci., Ser. C* **1971**, *272*, 206−208.
(25) Prakash, J.; Mesbah, A.; Ward, M. D.; Lebègue, S.; Malliakas, C. D.; Lee, M.; Choi, E. S.; Ibers, J. A. *Inorg. Chem.* **2015**, *54*, 1684−1689.
(26) Daoudi, A.; Lamire, M.; Levet, J. C.; Noël, H. *J. Solid State Chem.* **1996**, *123*, 331−336.
(27) Huang, F. Q.; Ibers, J. A. *J. Solid State Chem.* **2001**, *159*, 186−190.
(28) Oh, G. N.; Choi, E. S.; Ibers, J. A. *Inorg. Chem.* **2012**, *51*, 4224−4230.
(29) Ward, M. D.; Oh, G. N.; Mesbah, A.; Lee, M.; Choi, E. S.; Ibers, J. A. *J. Solid State Chem.* **2015**, *228*, 14−19.
(30) Malliakas, C. D.; Yao, J.; Wells, D. M.; Jin, G. B.; Skanthakumar, S.; Choi, E. S.; Balasubramanian, M.; Soderholm, L.; Ellis, D. E.; Kanatzidis, M. G.; Ibers, J. A. *Inorg. Chem.* **2012**, *51*, 6153−6163.
(31) Bugaris, D. E.; Choi, E. S.; Copping, R.; Glans, P.-A.; Minasian, S. G.; Tyliszczak, T.; Kozimor, S. A.; Shuh, D. K.; Ibers, J. A. *Inorg. Chem.* **2011**, *50*, 6656−6666.
(32) Mesbah, A.; Malliakas, C. D.; Lebègue, S.; Sarjeant, A. A.; Stojko, W.; Koscielski, L. A.; Ibers, J. A. *Inorg. Chem.* **2014**, *53*, 2899−2903.
(33) Mesbah, A.; Stojko, W.; Lebègue, S.; Malliakas, C. D.; Frazer, L.; Ibers, J. A. *J. Solid State Chem.* **2015**, *221*, 398−404.
(34) Yao, J.; Ibers, J. A. *Z. Anorg. Allg. Chem.* **2008**, *634*, 1645−1647.
(35) Bugaris, D. E.; Ibers, J. A. *Inorg. Chem.* **2012**, *51*, 661−666.
(36) Mesbah, A.; Lebegue, S.; Klingsporn, J. M.; Stojko, W.; Van Duyne, R. P.; Ibers, J. A. *J. Solid State Chem.* **2013**, *200*, 349−353.
(37) Zeng, H.-yi; Yao, J.; Ibers, J. A. *J. Solid State Chem.* **2008**, *181*, 552−555.
(38) Prakash, J.; Mesbah, A.; Lebègue, S.; Malliakas, C. D.; Ibers, J. A. *J. Solid State Chem.* **2015**, *230*, 70−74.
(39) Prakash, J.; Mesbah, A.; Beard, J.; Lebègue, S.; Malliakas, C. D.; Ibers, J. A. *Inorg. Chem.* **2015**, *54*, 3688−3694.
(40) Bugaris, D. E.; Ibers, J. A. *J. Solid State Chem.* **2008**, *181*, 3189−3193.
(41) Haneveld, A. J. K.; Jellinek, F. *J. Less-Common Met.* **1969**, *18*, 123−129.
(42) Huang, F. Q.; Mitchell, K.; Ibers, J. A. *Inorg. Chem.* **2001**, *40*, 5123−5126.
(43) Trok, R.; Zolnierek, Z. *J. Phys. (Paris)* **1979**, *40*, C4-79−C4-81.
(44) Jin, G. B.; Raw, A. D.; Skanthakumar, S.; Haire, R. G.; Soderholm, L.; Ibers, J. A. *J. Solid State Chem.* **2010**, *183*, 547−550.
(45) *Bruker APEX2 Version 2009.5-1; Data Collection and Processing Software*; Bruker Analytical X-Ray Instruments, Inc.: Madison, WI, USA, 2009.
(46) Sheldrick, G. M. *Acta Crystallogr., Sect. A: Found. Crystallogr.* **2008**, *64*, 112−122.
(47) Sheldrick, G. M. *SADABS*; Department of Structural Chemistry, University of Göttingen: Göttingen, Germany, 2008.
(48) Gelato, L. M.; Parthé, E. *J. Appl. Crystallogr.* **1987**, *20*, 139−143.
(49) Spek, A. L. *PLATON, A Multipurpose Crystallographic Tool*; Utrecht University: Utrecht, The Netherlands, 2014.
(50) Kresse, G.; Furthmüller, J. *Comput. Mater. Sci.* **1996**, *6*, 15−50.
(51) Kresse, G.; Joubert, D. *Phys. Rev. B: Condens. Matter Mater. Phys.* **1999**, *59*, 1758−1775.
(52) Kohn, W.; Sham, L. J. *Phys. Rev.* **1965**, *140*, A1133−A1138.
(53) Hohenberg, P.; Kohn, W. *Phys. Rev.* **1964**, *136*, B864−B871.
(54) Blöchl, P. E. *Phys. Rev. B: Condens. Matter Mater. Phys.* **1994**, *50*, 17953−17979.
(55) Heyd, J.; Scuseria, G. E.; Ernzerhof, M. *J. Chem. Phys.* **2003**, *118*, 8207−8215.
(56) Heyd, J.; Scuseria, G. E.; Ernzerhof, M. *J. Chem. Phys.* **2006**, *124*, 219906.
(57) Paier, J.; Marsman, M.; Hummer, K.; Kresse, G.; Gerber, I. C.; Angyan, J. G. *J. Chem. Phys.* **2006**, *124*, 154709.
(58) Strobel, S.; Schleid, T. *Z. Anorg. Allg. Chem.* **2002**, *628*, 2211.
(59) Chen, X.-a; Wada, H.; Sato, A.; Nozaki, H. *J. Alloys Compd.* **1999**, *290*, 91−96.
(60) Lu, Y.-J.; Ibers, J. A. *Inorg. Chem.* **1991**, *30*, 3317−3320.
(61) Yang, Y.; Ibers, J. A. *J. Solid State Chem.* **1999**, *147*, 366−371.
(62) Koscielski, L. A.; Ibers, J. A. *Acta Crystallogr., Sect. E: Struct. Rep. Online* **2012**, *68*, i52.
(63) D'Eye, R. W. M.; Sellman, P. G.; Murray, J. R. *J. Chem. Soc.* **1952**, *74*, 2555−2562.
(64) Sutorik, A. C.; Albritton-Thomas, J.; Hogan, T.; Kannewurf, C. R.; Kanatzidis, M. G. *Chem. Mater.* **1996**, *8*, 751−761.
(65) Lu, Y.-J.; Ibers, J. A. *J. Solid State Chem.* **1991**, *94*, 381−385.
(66) Mesbah, A.; Ibers, J. A. *J. Solid State Chem.* **2013**, *199*, 253−257.
(67) Yao, J.; Wells, D. M.; Chan, G. H.; Zeng, H.-Y.; Ellis, D. E.; Van Duyne, R. P.; Ibers, J. A. *Inorg. Chem.* **2008**, *47*, 6873−6879.
(68) Prakash, J.; Tarasenko, M. S.; Mesbah, A.; Lebègue, S.; Malliakas, C. D.; Ibers, J. A. *Inorg. Chem.* **2014**, *53*, 11626−11632.

DOI: 10.1021/acs.inorgchem.5b01566
Inorg. Chem. 2015, 54, 9138−9145